Functional Properties of the *Drosophila melanogaster* Inositol 1,4,5-Trisphosphate Receptor Mutants

Sonal Srikanth,*† Zhengnan Wang,* Huiping Tu,* Shalima Nair,† M. K. Mathew,† Gaiti Hasan,† and Ilya Bezprozvanny*

*Department of Physiology, University of Texas Southwestern Medical Center at Dallas, Dallas, Texas; and the †National Center for Biological Sciences, Tata Institute of Fundamental Research, Bangalore, India

ABSTRACT The inositol (1,4,5)-trisphosphate receptor ($InsP_3R$) is an intracellular calcium (Ca^{2+}) release channel that plays a crucial role in cell signaling. In *Drosophila melanogaster* a single $InsP_3R$ gene (*itpr*) encodes a protein ($DmInsP_3R$) that is ~60% conserved with mammalian $InsP_3Rs$. A number of *itpr* mutant alleles have been identified in genetic screens and studied for their effect on development and physiology. However, the functional properties of wild-type or mutant $DmInsP_3Rs$ have never been described. Here we use the planar lipid bilayer reconstitution technique to describe single-channel properties of embryonic and adult head $DmInsP_3R$ splice variants. The three mutants chosen in this study reside in each of the three structural domains of the $DmInsP_3R$—the amino-terminal ligand binding domain (ug3), the middle-coupling domain (wc703), and the channel-forming region (ka901). We discovered that 1), the major functional properties of $DmInsP_3R$ (conductance, gating, and sensitivity to $InsP_3$ and Ca^{2+}) are remarkably conserved with the mammalian $InsP_3R1$; 2), single-channel conductance of the adult head $DmInsP_3R$ isoform is 89 pS and the embryonic $DmInsP_3R$ isoform is 70 pS; 3), ug3 mutation affects sensitivity of the $DmInsP_3Rs$ to activation by $InsP_3$, but not their $InsP_3$-binding properties; 4), wc703 channels have increased sensitivity to modulation by Ca^{2+}; and 5), homomeric ka901 channels are not functional. We correlated the results obtained in planar lipid bilayer experiments with measurements of $InsP_3$-induced Ca^{2+} fluxes in microsomes isolated from wild-type and heterozygous *itpr* mutants. Our study validates the use of *D. melanogaster* as an appropriate model for $InsP_3R$ structure-function studies and provides novel insights into the fundamental mechanisms of the $InsP_3R$ function.

INTRODUCTION

The inositol (1,4,5)-trisphosphate receptor ($InsP_3R$) is an intracellular calcium (Ca^{2+}) release channel that plays a critical role in Ca^{2+} signaling (Berridge, 1993). Three mammalian isoforms of the $InsP_3R$—type I ($InsP_3R1$), type II ($InsP_3R2$), and type III ($InsP_3R3$)—have been identified (Furuichi et al., 1994). All three mammalian isoforms share a common domain structure and 60–70% sequence identity (Furuichi et al., 1994). The differences in functional properties between mammalian $InsP_3R$ isoforms are beginning to be elucidated (Miyakawa et al., 1999; Thrower et al., 2001). $InsP_3Rs$ are subjected to multiple levels of regulation (Berridge, 1993; Bezprozvanny and Ehrlich, 1995; Taylor, 1998). Structural determinants responsible for $InsP_3R1$ conductance and gating properties (Boehning et al., 2001; Ramos-Franco et al., 1999) and modulation by Ca^{2+} (Miyakawa et al., 2001; Nosyreva et al., 2002; Tu et al., 2003), ATP (Tu et al., 2002), and phosphorylation (Tang et al., 2003b; Wagner et al., 2003) have been uncovered in recent functional experiments with $InsP_3R1$ wild-type and mutant channels.

A single copy of the $InsP_3R$ gene (*itpr*) is present in the genome of *Drosophila* (Hasan and Rosbash, 1992; Yoshikawa et al., 1992), a model organism, that has been used widely for genetic screens (Myers et al., 2000). Sequence analysis reveals that the *Drosophila* $InsP_3R$ protein ($DmInsP_3R$) shares the same domain structure and ~60% sequence identity with mammalian $InsP_3R$ isoforms, with the highest level of conservation in the amino-terminal ligand binding and the carboxy-terminal channel regions. Thus, it is likely that analysis of the $DmInsP_3R$ mutant isoforms, identified in genetic screens (Deshpande et al., 2000; Joshi et al., 2004; Venkatesh and Hasan, 1997), will provide important insights into fundamental mechanisms of the $InsP_3R$ function. However, in the absence of information regarding the functional properties of the wild-type $DmInsP_3R$ isoforms, the interpretation of results obtained from $DmInsP_3R$ mutants are limited.

Here we describe the functional properties of two wild-type $DmInsP_3R$ splice variants (Sinha and Hasan, 1999) and three $DmInsP_3R$ mutants (*ug3*, *wc703*, and *ka901*) (Deshpande et al., 2000; Joshi et al., 2004). The mutant isoforms affect residues conserved among all known $InsP_3Rs$ (Joshi et al., 2004). For functional analysis of $DmInsP_3R$ we expressed $DmInsP_3R$ wild-type and mutants in sf9 cells by baculoviral infection and analyzed the properties of resulting channels in planar lipid bilayers. This is the same approach that we used previously for structure-function analysis of the mammalian $InsP_3R1$ (Nosyreva et al., 2002; Tang et al., 2003a, b; Tu et al., 2002, 2003). Our results indicate that the main functional properties of $InsP_3Rs$ are conserved in evolution from flies to mammals. Moreover, changes in the

Submitted January 14, 2004, and accepted for publication February 23, 2004.

Address reprint requests to Dr. Ilya Bezprozvanny, E-mail: ilya.bezprozvanny@utsouthwestern.edu or to Dr. Gaiti Hasan, E-mail: gaiti@ncbs.res.in.

0006-3495/04/06/3634/13 $2.00

doi: 10.1529/biophysj.104.040121

DmInsP$_3$R properties induced by mutations provide novel insights into fundamental mechanisms of InsP$_3$R function. We also demonstrate that functional properties observed in vitro correlate well with in vivo function of DmInsP$_3$R mutants by measurement of Ca^{2+} fluxes from wild-type and heterozygous mutant flies.

MATERIALS AND METHODS

Ca^{2+} release assay

A modified protocol from Bramley et al. (1990) was used. In brief, microsomes were prepared in the presence of 200 μM free Ca^{2+}, from either 75 wandering third-instar larvae or ~200 adult heads, obtained from the appropriate genotypes. The Canton-S strain (CS) was used for studying properties of the wild-type InsP$_3$R and all point mutants were generated in the background of this wild-type strain. The tissues were homogenized in TSHMo buffer (10 mM Tris pH 7.4, 0.25 M sucrose, 12 mM monothioglycerol, 10 mM sodium molybdate, 200 μM $CaCl_2$) and a mixture of protease inhibitors (1 mM PMSF, 10 μg/ml leupeptin, and 10 μM E64) by 10–12 strokes of a 15-ml glass Teflon homogenizer. The homogenate was centrifuged immediately at 20,000 *g* for 20 min at 4°C. The supernatant was recentrifuged at 109,000 *g* on a tabletop ultracentrifuge (Rotor TLA 45 of Beckman centrifuges, Beckman Coulter, Fullerton, CA) for 1 h. The pellet was resuspended in fresh Ca^{2+}-free TSHMo buffer and centrifuged again at 109,000 *g* for 20 min. The pellet was resuspended in 150 μl of Ca^{2+}-free TSHMo buffer and used for Ca^{2+} release assays and for protein estimation by the Bradford's method. Microsomes were made in parallel, in Ca^{2+}-free buffer and otherwise identical conditions, and added to the buffers used for determining the standard curve for Ca^{2+} for each individual experiment (see below for details of Ca^{2+}-EGTA standard curve). The endogenous leak rate of each microsomal vesicle's preparation was checked by a standard fluorescence assay (Mathew et al., 1982, data not shown) before using them in the Ca^{2+}-release assay. Only vesicles with minimal Ca^{2+} leak, measured over a period of 10 min, were used for the Ca^{2+} release assay. No obvious difference in the leak rates between wild-type and mutant vesicles was observed.

Membrane-impermeant Ca^{2+}-sensitive ratiometric fluorescent dye, Fura-2 (Molecular Probes, Eugene, OR) was prepared in calcium-free water. Steady-state fluorescence measurement was performed in a SPEX Fluorolog-2 spectrofluorometer (SPEX Industries, Edison, NJ) at 20°C so as to minimize nonspecific calcium leak. For each run, ~15 μg of adult head microsomes or ~50 μg of larval microsomal vesicles were added to 2 ml of assay buffer (20 mM Tris, pH 7.4 and 80 mM NaCl in calcium-free water) containing 5 μM Fura-2. Steady-state kinetics of Ca^{2+} release were measured at various concentrations of $InsP_3$ and quantified by plotting a standard curve, with known amounts of free Ca^{2+} using the standard Ca^{2+}-EGTA buffering system. To take into account the buffering capacity of the microsomes, the standard curve was obtained for each experiment in the presence of wild-type or mutant microsomes, made in parallel in Ca^{2+}-free buffer. For heparin-mediated inhibition studies, a nonratiometric dye, Fluo-4, was used at 5 μM concentration. To examine the amount of Ca^{2+} trapped in microsomal vesicles of all genotypes fluorescence measurements were done before and after the addition of 0.1% Triton X-100, which was used for disrupting the microsomal vesicles, in the presence of 2 μM Fura-2.

Expression of the DmInsP$_3$R in sf9 cells

Full-length embryonic DmInsP$_3$R coding sequence (Sinha and Hasan, 1999) was cloned into pFastBac1 expression vector (Invitrogen, Carlsbad, CA). The 5′ UTR of the DmInsP$_3$R clone was replaced with the Kozak sequence by polymerase chain reaction to generate the DmInsP$_3$R-pFastBac1 construct. The Nhe1(1415)/Nhe1(3210) fragment of the DmInsP$_3$R-pFastBac1 clone was replaced by the corresponding fragment from an adult head (AH) AH-DmInsP$_3$R clone (Sinha and Hasan, 1999) to yield the AH-DmInsP$_3$R-pFastBac1 construct. Recently described ka901 (G2630S), wc703 (G2117E), and ug3 (S224F) mutations (Joshi et al., 2004) were generated in the DmInsP$_3$R-pFastBac1 construct by megaprimer polymerase chain reaction or by using the QuikChange Site-Directed Mutagenesis kit (Stratagene, La Jolla, CA), and verified by sequencing. DmInsP$_3$R, AH-DmInsP$_3$R, ka901, wc703, and ug3 baculoviruses were generated and amplified using Bac-to-Bac system (Invitrogen) as described previously (Nosyreva et al., 2002; Tu et al., 2002). The DmInsP$_3$R wild-type and mutants were expressed in *Spodoptera frugiperda* (sf9) cells as previously described (Nosyreva et al., 2002; Tu et al., 2002). Expression of the DmInsP$_3$R in wild-type and mutant flies and sf9 cells was confirmed by Western blotting with the affinity purified anti-DmInsP$_3$R rabbit polyclonal antibody (IB-9075) raised against KLH-conjugated peptide CEQRKQKQ-RLGLLNTTANSLLPFQ derived from the DmInsP$_3$R sequence. Lysates from *D. melanogaster* larvae and adult heads were used as controls for the specificity of IB-9075 antibody (see Results).

Single-channel recordings and analysis of the DmInsP$_3$R activity

Recombinant DmInsP$_3$R wild-type and mutants expressed in sf9 cells were incorporated into the bilayer by microsomal vesicle fusion as previously described for InsP$_3$RI (Nosyreva et al., 2002; Tu et al., 2002). The *cis* chamber contained 250 mM HEPES-Tris, pH 7.35 and the *trans* chamber, which was held at virtual ground, contained 55 mM $Ba(OH)_2$, dissolved in 250 mM HEPES, pH 7.35. Single-channel conductance values of the DmInsP$_3$R were determined from the slope of a linear fit to unitary current amplitude versus transmembrane voltage data in the range between +10 mV and −30 mV. For calcium-dependence experiments, free Ca^{2+} concentration in the *cis* chamber was controlled in the range of 10 nM (pCa 8) to 10 mM (pCa 2) by mixture of 1 mM EGTA, 1 mM HEDTA, and variable concentrations of $CaCl_2$ or Ca-$HEPES_2$. To construct $InsP_3$- and Ca^{2+}-dependence curves for the DmInsP$_3$R, the determined values of P_o were averaged across several independent experiments at each $InsP_3$ or Ca^{2+} concentration. For $InsP_3$-dependence experiments the averaged values of P_o are presented as mean ± SE (n = number of independent experiments) and fit by equation $P_o([InsP_3]) = P_{max}[InsP_3]^n/([InsP_3]^n + k_{InsP3}^n)$ modified from Lupu et al. (1998), where P_{max} is a maximal P_o value, n is a Hill coefficient, and k_{InsP3} is the apparent affinity of the DmInsP$_3$R for $InsP_3$. For Ca^{2+}-dependence experiments the averaged values of P_o are presented as mean ± SE (n = number of independent experiments) and fit by the bell-shaped equation $P_o([Ca^{2+}]) = 4P_m k^n[Ca^{2+}]^n/((k^n + [Ca^{2+}]^n)(K^n + [Ca^{2+}]^n))$, modified from Bezprozvanny et al. (1991), where P_m is a parameter proportional to the maximal P_o value, n is a Hill coefficient, k is the apparent affinity of Ca^{2+} activating site, and K is the apparent affinity of Ca^{2+} inhibitory site (Tu et al., 2003). The parameters of the optimal fits to $InsP_3$- and Ca^{2+}-dependence are in the text.

^{3}H-InsP$_3$ binding assay

Scatchard analysis of ^{3}H-$InsP_3$ binding to the DmInsP$_3$R and ug3 microsomes was performed as previously described for InsP$_3$RI (Kaznacheyeva et al., 1998). Briefly, microsomes (20 μg protein) were incubated on ice with 10 nM ^{3}H-$InsP_3$ and variable amounts of nonlabeled $InsP_3$ (from 10 nM to 8 μM) in the binding buffer (50 mM Tris-HCl, pH 9.0, 1 mM EDTA, 1 mM DTT, 100 mM NaCl) and precipitated with 12.5% PEG and 1.2 mg/ml γ-globulin at 14,000 *g*. Precipitates were quickly washed with the binding buffer, dissolved in Soluene (PerkinElmer, Boston, MA) and their [^{3}H] content was determined by liquid scintillation counting. Nonspecific counts, determined in the presence of 25 μM unlabeled $InsP_3$, were subtracted from the total to yield specific binding. The binding affinity and the density of specific ^{3}H-$InsP_3$ binding sites was determined from the linear fit to the Scatchard plot. The specific activity of ^{3}H-$InsP_3$ used in this assay (Amersham Biosciences, Piscataway, NJ) was 45 Ci/mmol.

RESULTS

Ca^{2+} release properties of the $DmInsP_3R$ wild-type and mutants

The domain structure of the $InsP_3R$ (Mignery and Sudhof, 1990) is conserved between the $DmInsP_3R$ and mammalian $InsP_3R$ isoforms. Similar to mammalian $InsP_3Rs$, the $DmInsP_3R$ can be divided into an amino-terminal ligand binding ($DmInsP_3R$-N, M1-H650) domain, a carboxy-terminal channel-forming ($DmInsP_3R$-C, S2360-Q2829) domain, and a middle-coupling ($DmInsP_3R$-M, N651-W2359) domain (Fig. 1). Two alternate splice events (at positions 980 and 1390) were originally described for the embryonic and adult head (AH) forms of the $DmInsP_3R$ (Sinha and Hasan, 1999). From subsequent sequencing of genomic DNA of the *itpr* gene it is now clear that alternate splicing occurs only at residue 980 to give the two forms shown in Fig. 1, which differ by the nine-amino-acid insertion in the AH isoform. There is no intron near residue 1390, and consequently both forms are identical in this region and contain the sequence *GVGHSV*. A number of lethal $DmInsP_3R$ mutants were recently obtained by chemical mutagenesis using ethyl methane sulfonate (Deshpande et al., 2000). Among 14 lethal mutant alleles of the $DmInsP_3R$ obtained in the ethyl methane sulfonate screen, genomic DNA in the region of the open reading frame has recently been sequenced from seven alleles (Joshi et al., 2004). In this article we focus on three $DmInsP_3R$ point mutants (*ug3*, *wc703*, and *ka901*; see Fig. 1) in which the altered residues are conserved between all known $InsP_3Rs$ (Joshi et al., 2004).

To determine consequences of identified mutations for the $DmInsP_3R$ function, a series of $InsP_3$-induced Ca^{2+} release

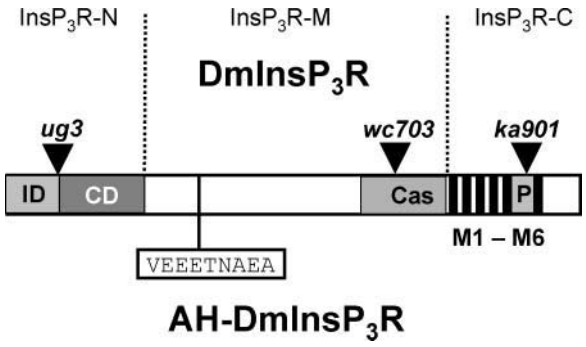

FIGURE 1 Schematic of the $DmInsP_3R$ showing point mutants used in this study. The amino-terminal ligand-binding domain ($DmInsP_3R$-N, M1-H650) consists of an inhibitory domain (*ID*, M1–E231) and the core-binding domain (*CD*, H232–H650). The middle-coupling domain ($DmInsP_3R$-M, N651–W2359) contains a site with a nine-amino-acid insertion in the adult head (*AH*) isoform in position E980 (Sinha and Hasan, 1999) and a putative Ca^{2+}-sensor region (Cas, G1986–S2354). The carboxy-terminal channel-forming domain ($DmInsP_3R$-C, S2360–Q2829) consists of M1–M6 transmembrane domains and a pore-forming region (*P*). Also shown are positions of three $DmInsP_3R$ point mutants identified in an ethyl methane sulfonate screen (Joshi et al., 2004), i.e., ug3 (S224F), wc703 (G2117E), and ka901 (G2630S).

experiments were performed with microsomes prepared from adult head and larval homogenates of wild-type and mutant flies. For generation of Ca^{2+}-loaded microsomal vesicles the buffer contained known amounts of free Ca^{2+} (Materials and Methods). Mutant vesicles were obtained from heterozygous flies, due to the fact that all homozygous mutant combinations are lethal. Since the functional $InsP_3$ receptor is a tetramer, in which interactions between monomers are known to affect Ca^{2+} release, it was reasoned that heterozygotes might exhibit mutant properties. In these experiments $DmInsP_3R$ function was quantified by measuring the $InsP_3$ concentration required to achieve half-maximal Ca^{2+}-release (K_m, nM $InsP_3$) and maximal amount of released Ca^{2+} (R_{max}, nmol Ca^{2+}/mg microsomal protein) values. As seen in Fig. 2 *A*, increasing amounts of $InsP_3$ showed an increase in fluorescence which was converted to the amount of Ca^{2+} released based on a calibration curve generated using a standard Ca-EGTA buffering system. The amount of Ca^{2+} released with increasing amounts of $InsP_3$ was seen to follow typical Michaelis-Menten kinetics (Fig. 2 *B*). We found that in wild-type organisms, the K_m values are similar in microsomes from larvae (405 $\pm$ 8 nM $InsP_3$) and adult heads (398 $\pm$ 14 nM $InsP_3$) (Fig. 2 *B*). In contrast, the R_{max} value is much higher in microsomes from adult heads (635 $\pm$ 42 nmol Ca^{2+}/mg protein) than from larvae (319 $\pm$ 22 nmol Ca^{2+}/mg protein; see Fig. 2 *B*). The K_m and R_{max} values were calculated as the average from at least three independent experiments. The graphs on Fig. 2 *B* show a single fit to the averaged data points.

The analysis of $DmInsP_3R$ mutants was carried out using AH microsomes, which release more Ca^{2+} (twofold higher R_{max}) than the larval microsomes (Fig. 2 *B*). Qualitatively similar results were obtained in experiments with microsomes from mutant larvae (data not shown). The specificity of the $InsP_3R$-mediated release in this assay was verified by using heparin, a competitive inhibitor of the $InsP_3R$. For this purpose, a nonratiometric dye, Fluo-4, was used. As seen in Fig. 2 *C*, $InsP_3$-mediated Ca^{2+} release is completely inhibited in the presence of 50 μg/ml of heparin. Microsomes isolated from the *ug3*/+ adult heads show a dominant phenotype of lowered K_m for $InsP_3$ (K_m = 274 $\pm$ 34 nM $InsP_3$) without affecting the R_{max} value (Fig. 2 *D*). Microsomes from adult heads of *wc703*/+ heterozygotes show an increased R_{max} (923 $\pm$ 29 nmol Ca^{2+}/mg protein; Fig. 2 *E*) but an unchanged K_m compared to wild-type (Fig. 2 *E*). Microsomes obtained from *ka901*/+ adult heads released over twice as much Ca^{2+} (R_{max} = 1678 $\pm$ 124 nmol Ca^{2+}/mg protein), with a significantly lower K_m (K_m = 308 $\pm$ 63 nM), compared to wild-type microsomes (Fig. 2 *F*).

From these experiments we concluded that each tested mutant allele has distinct Ca^{2+}-release properties in the Ca^{2+} flux assay. The observed changes in R_{max} could be due to different levels of the $DmInsP_3R$ protein among mutants or different amounts of Ca^{2+} trapped in vesicles from different genotypes. By Western blotting the levels of $DmInsP_3R$

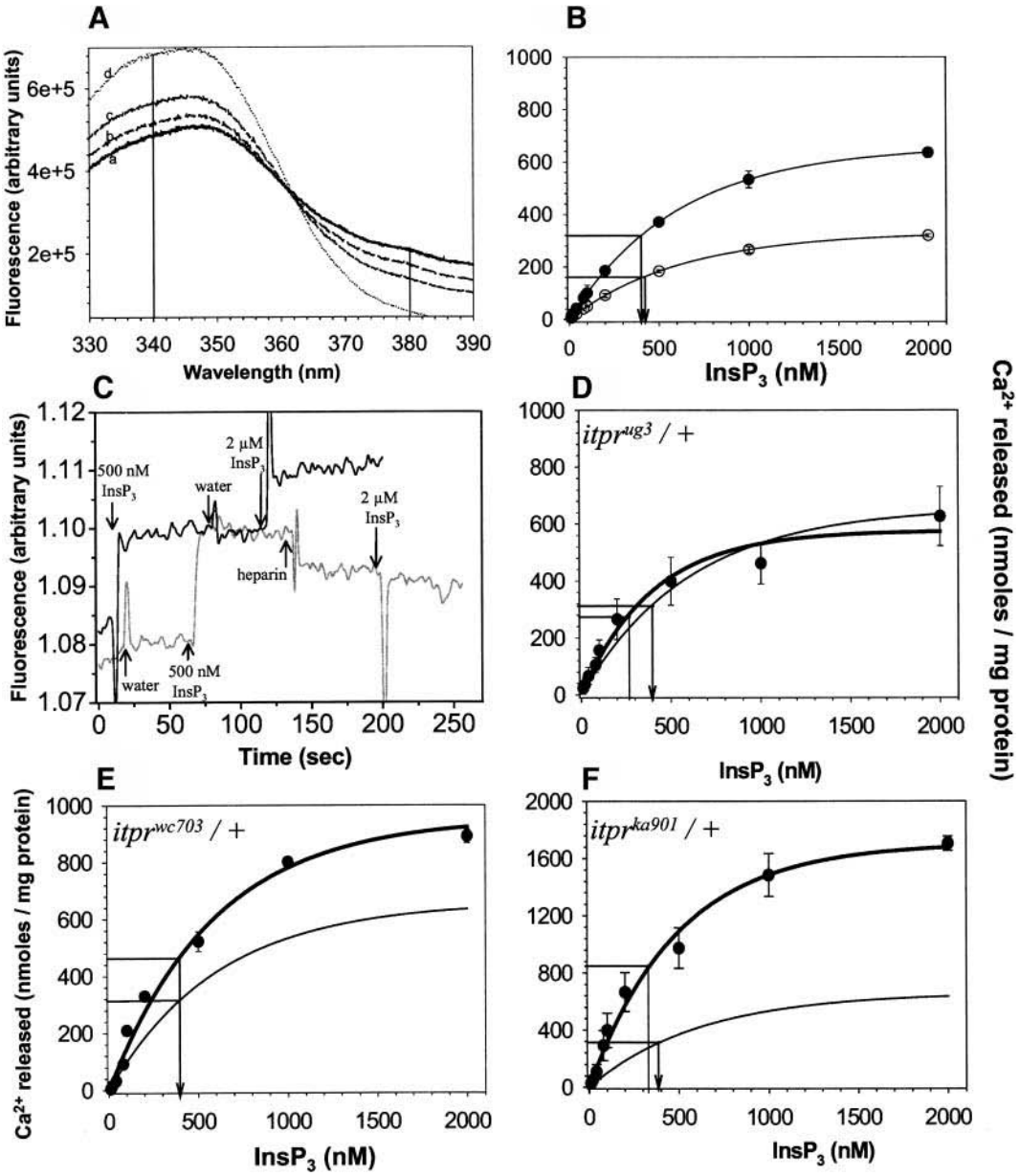

FIGURE 2 Ca^{2+} fluxes supported by the DmInsP$_3$R mutants. (*A*) Representative traces of Ca^{2+} release assay in microsomes isolated from the wild-type adult heads in the absence of InsP$_3$ (*trace a*) and in the presence of 20 nM (*trace b*), 200 nM (*trace c*), and 2 μM (*trace d*) InsP$_3$. The fluorescence values at 340 and 380 nm were utilized to calculate the amount of Ca^{2+} released (see Materials and Methods). Further, the free Ca^{2+} present without addition of InsP$_3$ (*trace a*) was subtracted from those with InsP$_3$ additions. (*B*) InsP$_3$-dependent Ca^{2+} fluxes in microsomal vesicles isolated from whole larvae (○) and adult heads (●) of the wild-type *Canton-S* (*CS*) strain. (*C*) Inhibition of InsP$_3$-mediated Ca^{2+} − release by heparin. Arrows indicate the time of addition of various reagents to microsomal vesicles in a buffer containing the fluorescent Ca^{2+} indicator dye Fluo-4. The two traces shown in black (− *heparin*) and gray (+ *heparin*) were obtained with the same batch of microsomes made from heads of the wild-type *CS* strain. The blips observed close to each arrow occur due to interference of the light beam by the syringe used to add reagents to the cuvette. Similar results have been observed independently with two other batches of microsomal vesicles. (*D–F*) InsP$_3$-dependent Ca^{2+} fluxes in microsomes isolated from adult heads (●) of *ug3*/+ (*D*), *wc703*/+ (*E*), and *ka901*/+ (*F*) flies. Wild-type adult head data from *B* are shown for comparison by the thin line in each graph. The difference in K_m between the wild-type and *ug3*/+ heterozygotes in *D* is statistically significant ($P < 0.001$). The concentrations of InsP$_3$ required for half-maximal Ca^{2+} release (K_m) are shown by arrowheads for wild-type and lines for mutants in *B* and *D–F*. All data in *B* and *D–F* are shown as the mean ± SD from at least three independent batches of microsomes. The data were fit to an exponential rise using SigmaPlot5 (SPSS, Chicago, IL).

protein were found to be equivalent in the wild-type and all mutant microsomes (Fig. 3 *A*). The amount of Ca^{2+} trapped in vesicles of all the genotypes was also found to be equivalent as determined by measuring Ca^{2+} release on addition of 0.1% Triton X-100 (Fig. 3 *B*). However, as expected from Fig. 2, *E* and *F*, the amount of $InsP_3$-releasable Ca^{2+} was found to be higher in vesicles from *itp*^{wc703} and *itpr*^{ka901} heterozygotes (Fig. 3 *B*). Therefore, the observed changes in R_{max} and K_m values most likely reflect changes in $DmInsP_3R$ functional properties induced by each mutation. To test this idea conclusively an alternate approach was adopted.

Single-channel properties of the $DmInsP_3R$ embryonic and adult head isoforms

Single-channel recordings offer by far the most detailed level of characterization of functional properties of channels. To obtain single-channel recordings of the $DmInsP_3R$, we adopted a previously described approach developed for the structure-functional analysis of the mammalian $InsP_3R1$ (Nosyreva et al., 2002; Tang et al., 2003a, b; Tu et al., 2002, 2003). The $DmInsP_3R$ (embryonic form) and AH-$DmInsP_3R$ (adult head form) were expressed in sf9 cells by baculovirus infection and the expression was confirmed by Western blotting (Fig. 4) using affinity-purified anti-$DmInsP_3R$ rabbit polyclonal antibodies. The apparent molecular weight of $DmInsP_3R$ and AH-$DmInsP_3R$ expressed in sf9 cells (280 kDa) was identical to endogenous $DmInsP_3R$ detected by the same antibodies in *Drosophila* larval and adult head lysates (Fig. 4). No signal was observed in samples prepared from noninfected sf9 cells (Fig. 4).

Recombinant $DmInsP_3R$ and AH-$DmInsP_3R$ expressed in sf9 cells were incorporated into the bilayer by microsomal vesicle fusion as described previously for the wild-type and mutant mammalian $InsP_3R1$ (Nosyreva et al., 2002; Tang et al., 2003a, b; Tu et al., 2002, 2003). $InsP_3$-gated currents supported by the $DmInsP_3R$ and the AH-$DmInsP_3R$ channels were recorded using 50 mM Ba^{2+} as the charge carrier at 0-mV holding potential (Fig. 5, *A* and *B*). $InsP_3$-gated channels in bilayers were observed in 45 of 50 experiments with $DmInsP_3R$ microsomes and in 40 of 50 experiments with AH-$DmInsP_3R$ microsomes, but were never ($n = 10$) observed in experiments with microsomes from noninfected sf9 cells. Single-channel analysis revealed that the mean current amplitude at 0-mV holding potential is equal to 1.80 ± 0.04 pA for the $DmInsP_3R$ (Fig. 5 *A*) and 1.86 ± 0.01 pA for the AH-$DmInsP_3R$ (Fig. 5 *B*); the mean open dwell time is equal to 4.3 ± 0.3 ms for the $DmInsP_3R$ (Fig. 5 *A*) and 3.6 ± 0.1 ms for the AH-$DmInsP_3R$ (Fig. 5 *B*) (Table 1).

To generate a current-voltage relationship, the transmembrane potential was varied between +10 mV and −30 mV during current recordings. A linear fit to the obtained results (Fig. 6) yielded single-channel conductances of 70.0 ± 0.1 pS for the $DmInsP_3R$ and 89.0 ± 0.1 pS for the AH-$DmInsP_3R$. From previous molecular analysis of these isoforms it is known that *Drosophila* larvae express both splice variants (predominantly the embryonic isoform) whereas only the AH form is present in adult heads. The higher conductance of the AH-$DmInsP_3R$ is thus consistent with the differences in R_{max} values observed between larval and adult head microsomes in the Ca^{2+}-release assay (Fig. 2 *B*).

To further characterize functional properties of the $DmInsP_3R$, its open probability was measured in a range of Ca^{2+} and $InsP_3$ concentrations. The analysis of the $DmInsP_3R$ $InsP_3$-sensitivity (Fig. 7) yielded an apparent affinity for $InsP_3$ equal to 100 nM. We found that similar to mammalian $InsP_3R1$ (Table 1), $DmInsP_3R$ displays a bell-

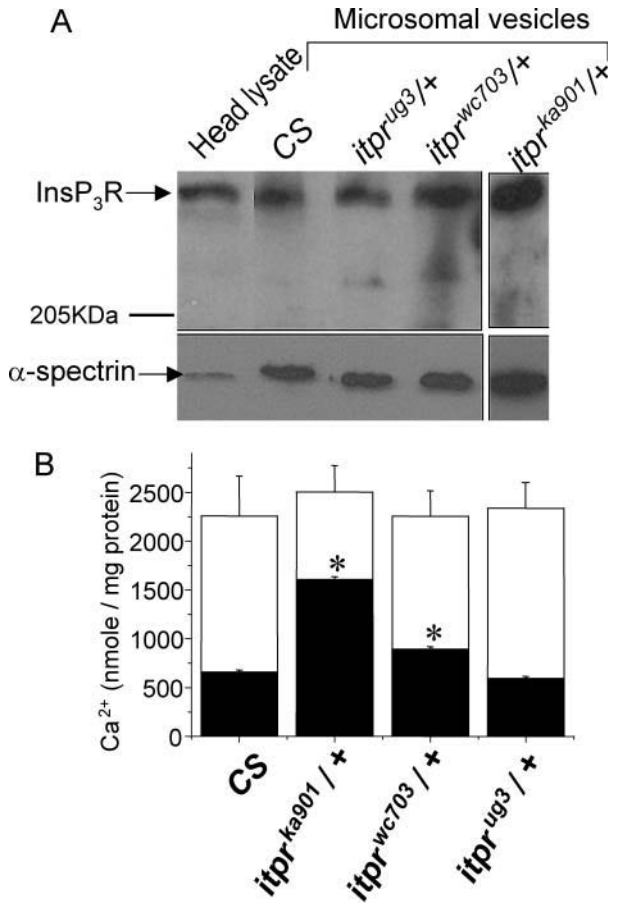

FIGURE 3 Levels of the $DmInsP_3R$ protein and Ca^{2+} in wild-type and mutant vesicles. (*A*) Western blot of wild-type and mutant adult head microsomes with anti-$DmInsP_3R$ polyclonal antibody. Lane 1, *CS* adult head lysate; lanes 2–5, microsomal vesicles from adult heads of the genotypes as indicated. Five micrograms of total protein was loaded in each lane. The blot was stripped and reprobed with antiserum to α-spectrin (278 kDa) as a loading control. When levels of the $DmInsP_3R$ were compared with the levels of the loading control by densitometry analysis, no significant changes were observed between the various genotypes. The representative blot of three independent experiments is shown. (*B*) Fraction of maximal Ca^{2+} released from microsomes in response to 2 μM $InsP_3$ (*black bars*) as a fraction of total vesicular Ca^{2+} (estimated by lysing the microsomes with 0.1% Triton X-100, *open bars*). The fraction of $InsP_3$-releasable Ca^{2+} was significantly higher in *itprwc703*/+ and *itprka901*/+ ($P < 0.001$ for both) microsomes than in wild-type (*CS*).

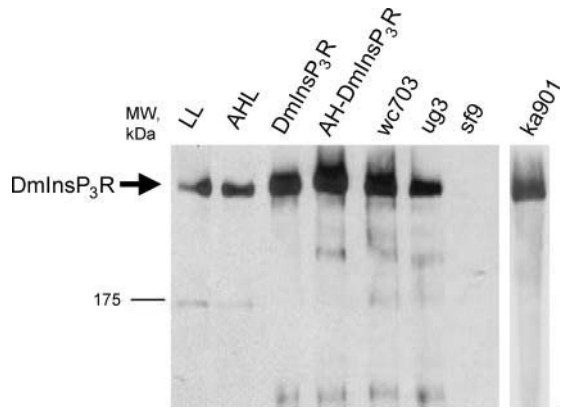

FIGURE 4 Expression of the DmInsP$_3$R in sf9 cells. Western blot of *Drosophila* larval (*LL*) and adult head (*AHL*) lysates and microsomes isolated from noninfected sf9 cells (*sf9*) and sf9 cells infected with DmInsP$_3$R, AH-DmInsP$_3$R, ug3, wc703, and ka901 baculoviruses as indicated. The DmInsP$_3$R was detected using an affinity-purified anti-DmInsP$_3$R polyclonal antibody. For the larval lysate 30 μg of total protein was loaded whereas 20 μg was loaded in the lane containing the adult head lysate. For each microsomal preparation, 100 ng of total microsomal protein was loaded on the gel except for ug3, where 300 ng total microsomal protein was loaded. The representative blot of three independent experiments is shown.

shaped Ca^{2+} dependence with the peak at pCa 6.4 (Fig. 8). On an average, the single-channel open probability of the DmInsP$_3$R channels at pCa 6.4 was equal to 0.15 $\pm$ 0.015. A fit to the averaged Ca^{2+}-dependence data (Fig. 8 *B*) using a modified bell-shaped equation from Bezprozvanny et al. (1991) yielded the affinities of activating and inhibitory sites of the DmInsP$_3$R equal to 0.28 μM Ca^{2+} and 0.53 μM Ca^{2+}, respectively. Although the affinity of the activating site is similar to mammalian InsP$_3$R1 (Nosyreva et al., 2002; Tu et al., 2002, 2003), the affinity for the inhibitory site is lower in the DmInsP$_3$R (Table 1), indicating that higher concentrations of cytoplasmic Ca^{2+} are required for inhibition of the InsP$_3$R in *Drosophila*. Similar results were obtained for the AH-DmInsP$_3$R (data not shown).

Functional properties of the ug3 mutant

To characterize single-channel properties of the ug3 mutant (embryonic form) it was expressed in sf9 cells by baculovirus infection. The expression levels of ug3 mutant channels in sf9 cells were lower than expression levels of the wild-type channels (in Fig. 4, a three-times excess of ug3 microsomes was loaded). When microsomes isolated from ug3-infected sf9 cells were fused to planar lipid bilayers, InsP$_3$-gated channels were observed less frequently than in experiments with wild-type microsomes (in 20 of 34 experiments; Fig. 9). The mean current amplitude of ug3 channels at 0-mV holding potential is 1.7 $\pm$ 0.32 pA (Fig. 9), with a mean open dwell time of 6.4 $\pm$ 0.8 ms (Fig. 9), and single-channel conductance of 71.0 $\pm$ 0.2 pS ($n = 3$, data not shown). Thus, ug3 channels display conductance properties similar to the wild-type DmInsP$_3$R (embryonic form), but have 47% longer mean open time.

The amino-terminal region of the InsP$_3$R forms a ligand-binding domain (Fig. 1). Biochemical and structural studies of mammalian InsP$_3$R1 indicate that the InsP$_3$R ligand-binding domain can be subdivided into a core InsP$_3$ binding domain and an inhibitory domain (Bosanac et al., 2002; Yoshikawa et al., 1999, 1996; see also Fig. 1, this article).

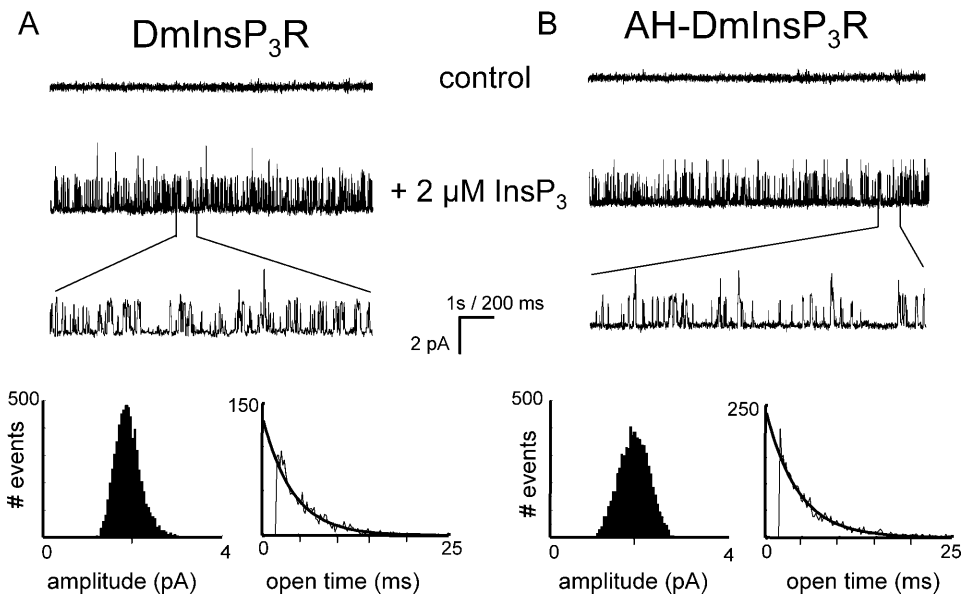

FIGURE 5 Functional properties of the wild-type isoforms of the DmInsP$_3$R. Representative channel activity of the DmInsP$_3$R (*A*) and the AH-DmInsP$_3$R (*B*) recorded in the presence of 0.2 μM Ca^{2+}, 0.5 mM Na_2ATP, and 2 μM InsP$_3$ (*standard recording conditions*). Current records are shown at compressed and expanded timescales as indicated. Unitary current amplitude histograms and open dwell time distributions from the same experiments are shown below the current records. Unitary currents were fitted with a Gaussian function that was centered at 1.83 pA for the DmInsP$_3$R and at 1.86 pA for the AH-DmInsP$_3$R. Open time distributions were fit with a single exponential function (*curve*) that yielded a τ_0 of 4.0 ms for the DmInsP$_3$R and 3.98 ms for the AH-DmInsP$_3$R. Similar analysis was performed for at least five independent experiments with the DmInsP$_3$R and the AH-DmInsP$_3$R microsomes.

TABLE 1 Comparison of main functional properties of DmInsP$_3$R and mammalian InsP$_3$R1 (Tang et al., 2003b; Tu et al., 2002)

		Conductance properties		Gating properties		InsP$_3$-dependence		Bell-shaped Ca^{2+} dependence			
InsP$_3$R isoform	Splice variant	i, pA	γ, pS	τ_o, ms	P_o max %	k_d, nM	n_{Hill}	n_{Hill}	K_{act}, μM	K_{inh}, μM	Peak (pCa)
InsP$_3$R1	SII(+)	1.9 pA	81 pS	4.7 ms	19%	190 nM	1.47	1.3	0.22 μM	0.20 μM	6.6
DmInsP$_3$R	emb	1.8 pA	70 pS	4.3 ms	15%	100 nM	1.13	0.91	0.28 μM	0.53 μM	6.4
DmInsP$_3$R	AH	1.9 pA	89 pS	3.6 ms	17%	ND			Similar to embryonic		
wc703	emb	1.75 pA	70 pS	4.5 ms	21%	ND		1.96	0.17 μM	0.18 μM	6.8
ug3	emb	1.72 pA	71 pS	6.4 ms	17%	ND			Similar to embryonic		

Sequences corresponding to the core and inhibitory domains are highly conserved between DmInsP$_3$R and InsP$_3$R1, and the ug3 mutation (S224F) is interestingly located at the interface between the predicted inhibitory and core domains of the DmInsP$_3$R (Fig. 1). From the position of the ug3 mutation in the ligand-binding domain it was expected that ug3 may have an effect on the binding affinity of the DmInsP$_3$R for InsP$_3$. Binding of ^{3}H-InsP$_3$ to microsomes isolated from the DmInsP$_3$R- and ug3-infected sf9 cells yielded affinity values of 152 nM InsP$_3$ for the wild-type DmInsP$_3$R (embryonic form) and 214 nM InsP$_3$ for the ug3 mutant (Fig. 10). The observed difference in affinity was found to be insignificant upon repetition of the experiment (data not shown). Notably, the affinity for InsP$_3$ is either the same or slightly lower in ug3 when compared with wild-type DmInsP$_3$R in ^{3}H-InsP$_3$ binding experiments (Fig. 10). This conclusion contrasts with higher sensitivity of *ug3*/+ microsomes to InsP$_3$ in the Ca^{2+} flux assay as compared to the wild-type microsomes (Fig. 2 *D*).

To understand this discrepancy, the sensitivity of ug3 channels to activation by low InsP$_3$ concentrations was investigated in bilayer experiments. We discovered that ug3 channels displayed maximum open probability (P_o) at InsP$_3$ concentrations as low as 50 nM (Fig. 11, *A* and *B*). Much higher concentrations of InsP$_3$ are required to fully activate the wild-type DmInsP$_3$R (Fig. 11, *C* and *D*, and Fig. 7). The ug3 channels are expressed in sf9 cells at a much lower level than DmInsP$_3$R. This was evident from the B_{max} values (180 pmol/mg for DmInsP$_3$R versus 124 pmol/mg for ug3 mutant) and the significantly lower abundance of the InsP$_3$R positive band in ug3 microsomes, as seen in a quantitative Western blot (Fig. 4, data not shown). Because of reduced expression levels of ug3 mutant and resulting difficulties with channel recordings, we have not been able to obtain a complete InsP$_3$-dependence curve for this mutant in planar lipid bilayers. However, it is clear from Fig. 11 that, unlike the DmInsP$_3$R, the open probability for ug3 is similar at 50 nM and 2 μM InsP$_3$, indicating a shift in apparent sensitivity to activation by InsP$_3$.

Functional properties of the wc703 mutant

To characterize single-channel properties of the wc703 mutant, its embryonic form was expressed in sf9 cells by baculovirus infection. The expression levels of the wc703

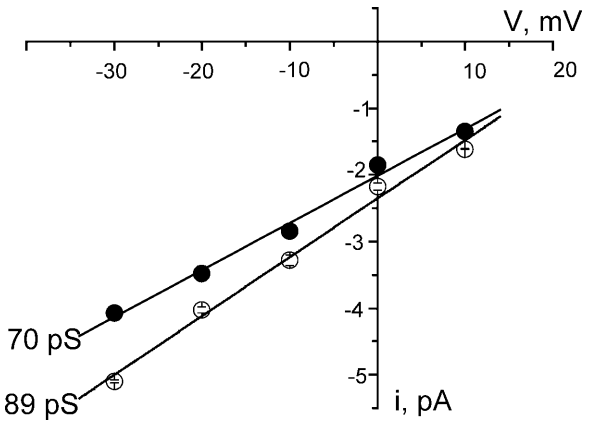

FIGURE 6 Current-voltage relationship of the DmInsP$_3$R isoforms. Current-voltage relationship of the DmInsP$_3$R (●) and the AH-DmInsP$_3$R (○) channels measured at transmembrane voltages between +10 mV and −30 mV. Average data from at least four independent experiments with DmInsP$_3$R and AH-DmInsP$_3$R are shown as the mean ± SE at each voltage. The linear fit to the data (*lines*) yielded single-channel conductance of 70.0 pS for the DmInsP$_3$R and 89 pS for the AH-DmInsP$_3$R.

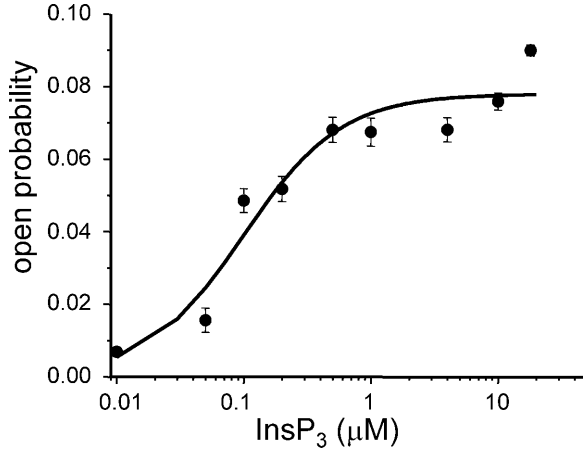

FIGURE 7 InsP$_3$ dependence of the DmInsP$_3$R. The DmInsP$_3$R Po measured in three independent experiments were averaged together at each InsP$_3$ concentration as described in Materials and Methods and shown as mean ± SE (●). The averaged data were fitted by the equation modified from Lupu et al. (1998) as explained in Materials and Methods. The parameters of optimal fit (*smooth curve*) yielded k_{InsP3} = 100 nM, n_{Hill} = 1.13, and P_{max} = 0.078.

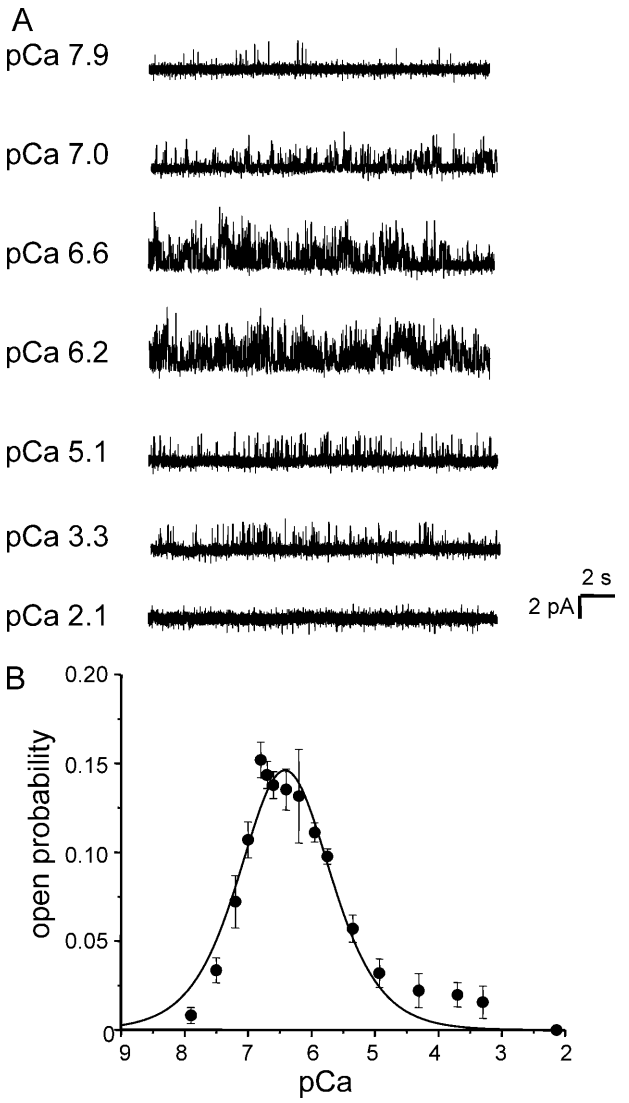

FIGURE 8 Calcium dependence of the DmInsP$_3$R. (*A*) Current recordings of the DmInsP$_3$R from the same experiment at different Ca^{2+} concentration as indicated. (*B*) Bell-shaped Ca^{2+} dependence of DmInsP$_3$R. The P_o measured in five independent experiments with DmInsP$_3$R were averaged together at each Ca^{2+} concentration as described in Materials and Methods and shown as mean ± SE (●). The averaged data were fitted by the bell-shaped equation modified from Bezprozvanny et al. (1991) as explained in Materials and Methods. The optimal fit (*smooth curve*) was obtained with $n_{Hill} = 0.91$, $P_m = 0.13$, $k_{act} = 0.28$ μM Ca^{2+}, and $K_{inh} = 0.53$ μM Ca^{2+}.

mutant in sf9 cells were comparable to expression levels of the wild-type channels (Fig. 4). When microsomes isolated from the wc703-infected sf9 cells were fused to planar lipid bilayers, InsP$_3$-gated channels were observed in 25 of 40 experiments (Fig. 12 *A*). Thus, similar to the ug3 mutant, homomeric channels formed by wc703 mutant subunits are functional. The mean current amplitude of wc703 channels at 0-mV holding potential is 1.74 ± 0.08 pA (Fig. 12 *A*), with a mean open dwell time of 4.5 ± 0.4 ms (Fig. 12 *A*), and single-channel conductance of 69.0 ± 0.1 pS ($n = 3$, data not shown). Thus, gating and conductance properties of wc703 channels are not significantly different from the wild-type DmInsP$_3$R (embryonic form). To determine the effect of wc703 mutation on Ca^{2+} sensitivity of the DmInsP$_3$R, we measured open probability of wc703 channels in bilayers at different Ca^{2+} concentrations. We discovered that, in contrast to the wild-type DmInsP$_3$R, the maximal open probability of wc703 was achieved at pCa 6.8 (Fig. 12 *B*). On an average, the single-channel open probability of wc703 channels at pCa 6.8 was equal to 0.21 ± 0.013. Fit to the averaged Ca^{2+}-dependence data (Fig. 12 *C*, $n = 3$) using a modified bell-shaped equation from Bezprozvanny et al. (1991) yielded the affinities of activating and inhibitory sites of DmInsP$_3$R equal to 0.17 μM Ca^{2+} and 0.18 μM Ca^{2+}, respectively. The observed effects on the DmInsP$_3$R Ca^{2+} sensitivity are consistent with the position of the wc703 mutation (G2117E) in a Ca^{2+}-sensor region (Tu et al., 2003) of the DmInsP$_3$R (Fig. 1). The results suggest that the increased R_{max} observed in the Ca^{2+}-release assay with microsomes from *wc703*/+ flies (Fig. 2 *E*) can be explained by the approximately twofold increase in an apparent affinity of DmInsP$_3$R Ca^{2+} sensor and 30% increase in the DmInsP$_3$R maximal single-channel open probability.

Absence of channel function in the ka901 mutant

The DmInsP$_3$R ka901 mutant (embryonic form) was expressed in sf9 cells by baculovirus infection. As determined by Western blotting, expression levels of ka901 in sf9 cells were comparable to expression levels of wild-type channels (Fig. 4). However, InsP$_3$-gated channel activity was not observed in bilayer experiments with microsomes from ka901-infected sf9 cells ($n = 15$), indicating that ka901 homomeric channels are nonfunctional. This idea is supported by the observation that ka901 mutants are equivalent to null alleles of the InsP$_3$R in *Drosophila* (Joshi et al., 2004). Interestingly, however, we did measure increased Ca^{2+} fluxes in microsomes from *ka901*/+ flies (Fig. 2 *F*). Taken together, these observations suggest that ka901 may form functional channels when assembled with the wild-type DmInsP$_3$R subunits, but not in the homomeric state.

DISCUSSION

Major functional properties of InsP$_3$Rs are conserved in evolution

The major functional properties of embryonic and adult head splice variants of the *Drosophila* InsP$_3$R obtained from planar lipid bilayer experiments (Figs. 5–8) have been described here. To the best of our knowledge, this is the first description of single-channel properties of *Drosophila melanogaster* InsP$_3$R. On comparison with the properties of rat InsP$_3$R1, determined in identical experimental conditions in our previous studies (Tang et al., 2003b; Tu

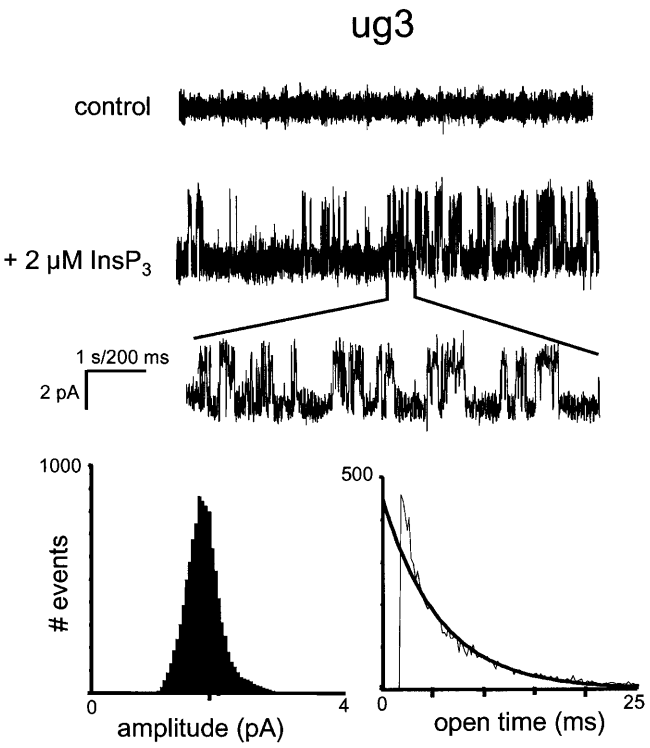

FIGURE 9 Functional properties of ug3 channels. Representative channel activity of ug3 channels recorded in the standard recording conditions. Current records are shown at compressed and expanded timescales as indicated. Unitary current amplitude histograms and open dwell time distributions from the same experiments are shown below the current records. Unitary current distribution was fit with a Gaussian function that was centered at 1.71 pA. Open time distribution was fit with a single exponential function (*curve*) that yielded a τ_0 of 5.6 ms. Similar analysis was performed for at least three independent experiments with ug3 microsomes.

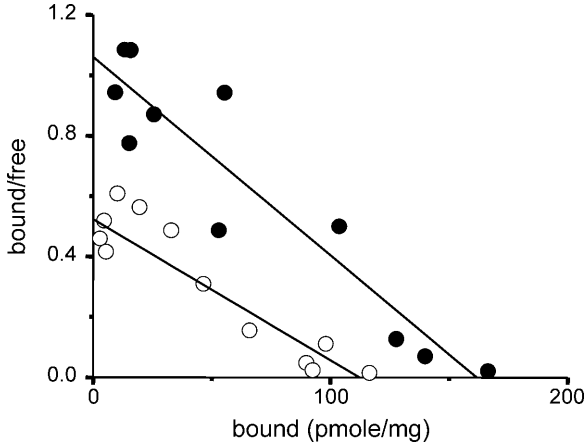

FIGURE 10 ^{3}H-InsP$_3$ binding studies with the DmInsP$_3$R and ug3 microsomes. Scatchard analysis of ^{3}H-InsP$_3$ binding to the DmInsP$_3$R (●) and ug3 (○) microsomes. Linear fit to the data (*lines*) yielded $k_d = 152$ nM InsP$_3$ and $B_{max} = 180$ pmol/mg for the DmInsP$_3$R and $k_d = 214$ nM InsP$_3$ and $B_{max} = 124$ pmol/mg for the ug3 mutant. The experiment was repeated in duplicate with similar results.

et al., 2002), we conclude that the single-channel properties of the DmInsP$_3$R are remarkably similar to the single-channel properties of mammalian InsP$_3$R1, apart from a broader Ca^{2+}-dependence curve (Table 1). This conclusion agrees with the conservation of InsP$_3$R domain structure (Fig. 1), and the high degree of sequence identity (57%) between DmInsP$_3$R and rat InsP$_3$R1, and with previous analysis of InsP$_3$-dependent Ca^{2+} fluxes in *Drosophila*-derived S2 cells (Swatton et al., 2001). Overall, our results validate the use of *Drosophila* as a genetic model for InsP$_3$R structure-function analysis, as results obtained with the DmInsP$_3$R are likely to have an implication for understanding the mechanisms of mammalian InsP$_3$R function. Interestingly, an SIII splice variant of the human type I InsP$_3$R, spliced in a region homologous to the *Drosophila* adult head isoform, is enriched in brain tissues (Nucifora et al., 1995). This SIII splice variant contains nine additional amino acids, which give rise to a putative protein kinase C phosphorylation site. The nine-amino-acid insert in the fly adult head isoform also contains a putative casein kinase II phosphorylation site. It would thus be interesting to compare the single-channel properties of the SIII isoform of human InsP$_3$RI with the adult head isoform of DmInsP$_3$R described here.

DmInsP$_3$R ug3—the InsP$_3$ efficacy mutant

The ug3 mutation (S224F) is located within the ligand-binding domain of DmInsP$_3$R (Fig. 1). Thus the observation that ug3 affects the InsP$_3$ sensitivity of DmInsP$_3$R channel opening (Fig. 11, *A–D*), but does not increase InsP$_3$ binding affinity (Fig. 10), is intriguing. This result suggests that the InsP$_3$R inhibitory domain plays an important role in coupling InsP$_3$ binding to the core domain with opening of the InsP$_3$R channel gate, in agreement with recent biochemical (Boehning and Joseph, 2000) and functional (Uchida et al., 2003) data. Increased open dwell time in ug3 mutants (by 47%) is consistent with the conclusion that ug3 is not a binding mutant, but is, in fact, a gating mutant. These data lead us to conclude that the increased apparent affinity to InsP$_3$ (change in K_m) observed in Ca^{2+} flux assay with *ug3*/+ microsomes (Fig. 2 *D*) results not from an increased affinity of the DmInsP$_3$R for InsP$_3$ but from an increased efficacy in coupling InsP$_3$ binding with DmInsP$_3$R channel opening. Thus, ug3 is a gain-of-function mutant that acts by increasing sensitivity of the DmInsP$_3$R to activation by InsP$_3$ and also by increasing dwell open time of the channels. Since the affinity of InsP$_3$ binding is not increased by the ug3 mutation (Fig. 10), we classified the ug3 mutant as the *efficacy mutant*, that is, the mutant with increased efficiency of coupling between InsP$_3$ binding and channel opening. This conclusion is consistent with the biochemical association observed between InsP$_3$R1 amino-terminal and carboxy-terminal ends (Boehning and Joseph, 2000) and a recent suggestion that the InsP$_3$R1 inhibitory

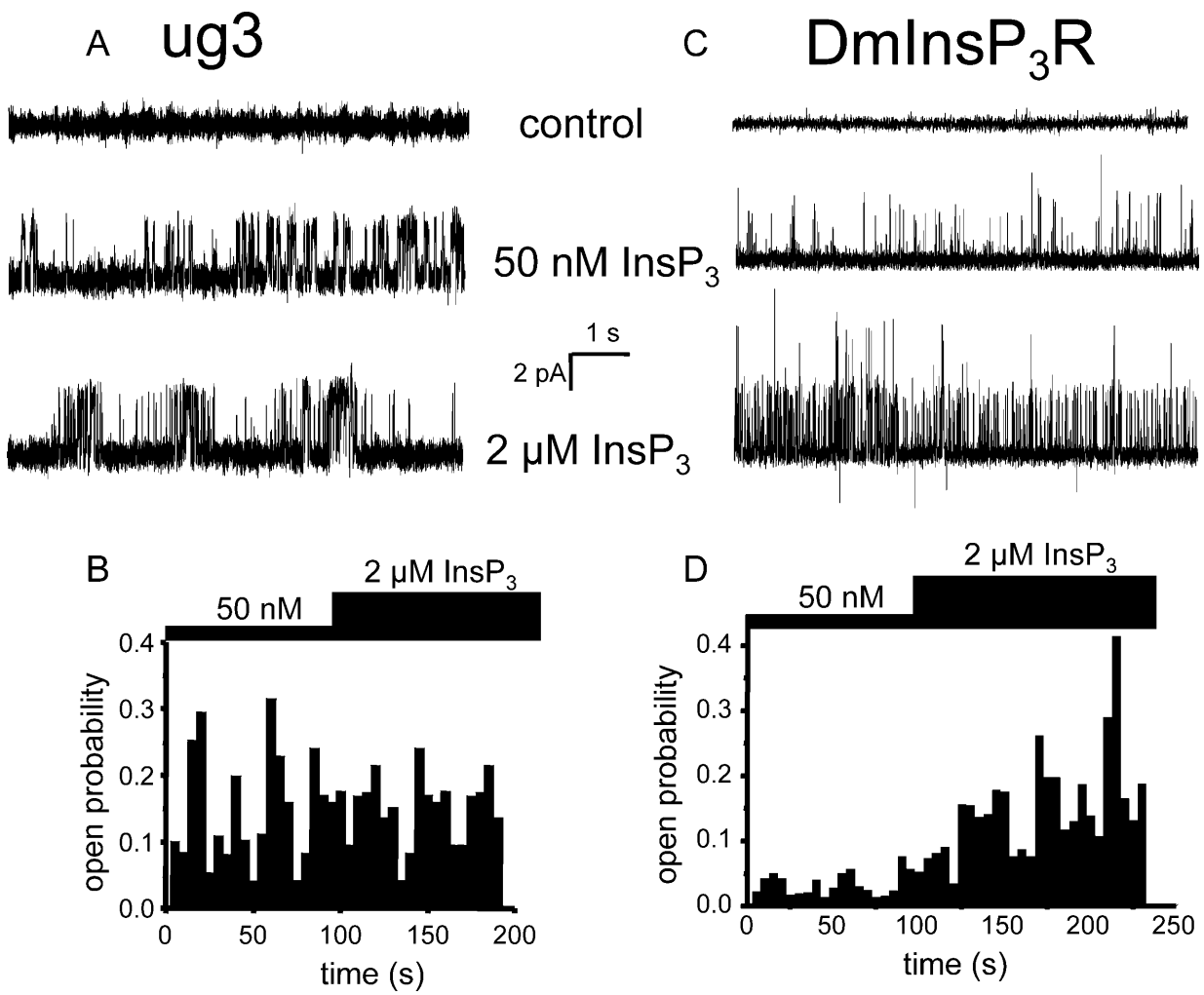

FIGURE 11 InsP$_3$ sensitivity of ug3 channels. (*A*) Activity of ug3 channels in bilayers in the presence of 50 nM InsP$_3$ and 2 μM InsP$_3$ is shown. Each current trace corresponds to 10 s of current recording from the same experiment. (*B*) The average open probability (P_o) of ug3 channels is calculated for a 5-s window of time and plotted for the duration of an experiment. The times of 50 nM and 2 μM InsP$_3$ additions to the bilayer are shown above the P_o plot. Data from the same experiment are shown in *A* and *B*. Similar results were obtained in three independent experiments. (*C–D*) Same data as in *A* and *B* for the wild-type DmInsP$_3$R channels. Similar results were obtained in three independent experiments.

amino-terminal domain participates in the channel-gating process (Uchida et al., 2003).

The observation that ug3 homomeric channels are functional is consistent with the weak allelic strength of *ug3* mutants. Heterozygotes of the genotype *ug3/90B0* die as late second- or early third-instar larvae (Deshpande et al., 2000; Joshi et al., 2004) as compared to *ka901/90B0* and *90B0/90B0* (*itpr* null) mutants, both of which die as early second-instar larvae (Venkatesh and Hasan, 1997).

DmInsP$_3$R wc703—the Ca^{2+} sensor mutant

Microsomes from *wc703/+* flies display increased Ca^{2+} release (1.4-fold increase in R_{max}) in Ca^{2+} flux experiments (Fig. 2 *E*). Although single channels formed by wc703 display wild-type conductance and gating properties (Fig. 12 *A* and data not shown), they also exhibit increased sensitivity to Ca^{2+} and a higher maximal open probability (Fig. 12, *B* and *C*, and Table 1). The peak of wc703 channel Ca^{2+} dependence is at pCa 6.8 (compare to pCa 6.4 for wild-type channels) and their maximal open probability is 21% (as compared to 15% for wild-type). A fit of the bell-shaped Ca^{2+} dependence of wc703 channels yielded affinities of activating and inhibitory Ca^{2+} binding sites equal to 0.17 μM Ca^{2+} and 0.18 μM Ca^{2+}, respectively (as compared to 0.28 μM Ca^{2+} and 0.53 μM Ca^{2+} for the wild-type DmInsP$_3$R). These results indicate that wc703 is also a gain-of-function mutant that acts by increasing sensitivity of DmInsP$_3$R to activation by Ca^{2+}. These effects are consistent with the position of wc703 mutation (G2117E) within a putative Ca^{2+} sensor region (Tu et al., 2003) of the DmInsP$_3$R (Fig. 1). The wc703 homomeric channels are functional, consistent with the weak allelic strength of *wc703*

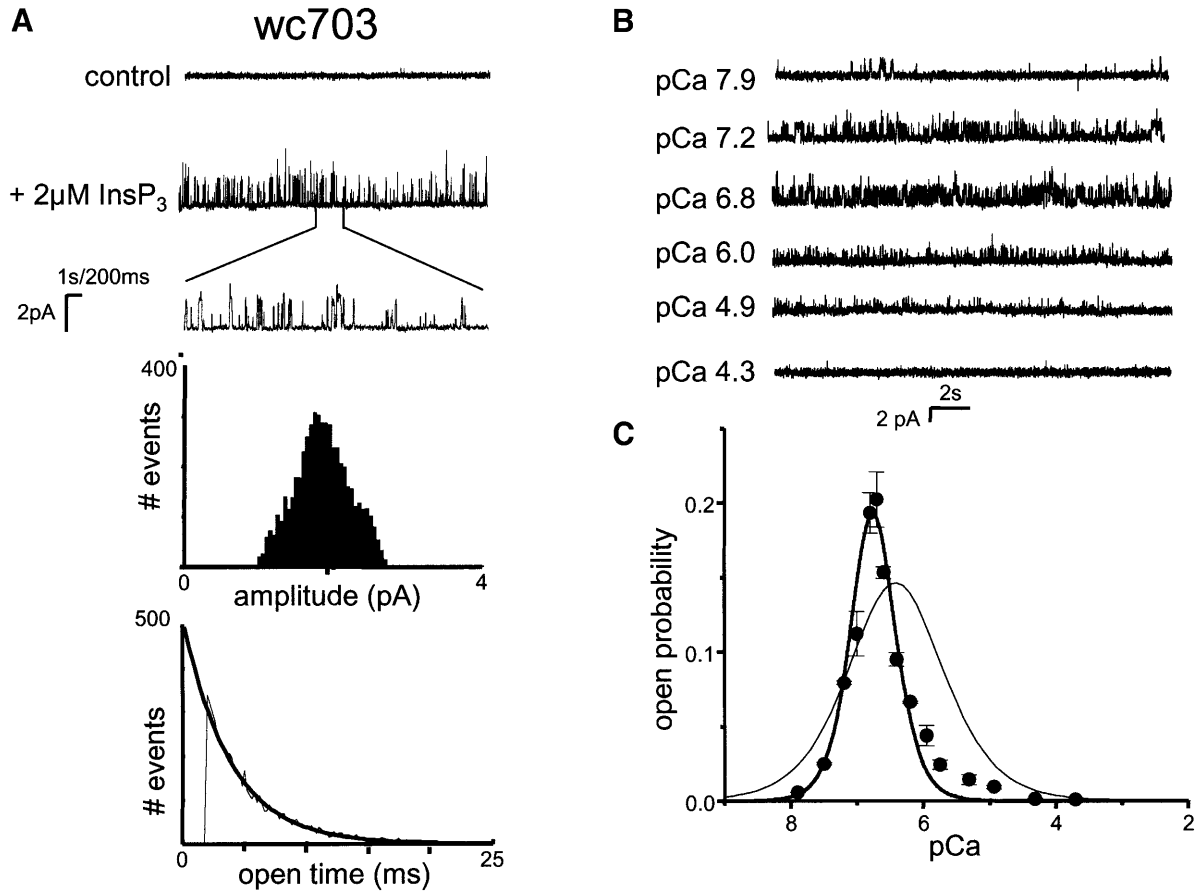

FIGURE 12 Functional properties of wc703 channels. (*A*) Representative channel activity of wc703 channels recorded in the standard recording conditions. Current records are shown at compressed and expanded timescales as indicated. Unitary current amplitude histograms and open dwell time distributions from the same experiments are shown below the current records. Unitary current distribution was fit with a Gaussian function that was centered at 1.82 pA. Open time distribution was fit with a single exponential function (*curve*) that yielded a τ_0 of 3.8 ms. Similar analysis was performed for at least four independent experiments with wc703 microsomes. (*B*) The current recordings of wc703 from the same experiment at different Ca^{2+} concentration as indicated. (*C*) Bell-shaped Ca^{2+} dependence of wc703. The P_o measured in three independent experiments with wc703 were averaged together at each Ca^{2+} concentration as described in Materials and Methods and shown as mean ± SE (●). The averaged data were fitted by the bell-shaped equation modified from Bezprozvanny et al. (1991) as explained in Materials and Methods. The optimal fit (*thick smooth curve*) was obtained with $n_{Hill} = 1.9$, $P_m = 0.2$, $k_{act} = 0.17$ μM Ca^{2+}, and $K_{inh} = 0.18$ μM Ca^{2+}. The fit to the Ca^{2+} dependence of the wild-type $DmInsP_3R$ (embryonic form) from Fig. 8 is shown for the reference (*thin line*).

mutants, which is similar to that of the *ug3* allele (Deshpande et al., 2000; Joshi et al., 2004).

$DmInsP_3R$ ka901—the Ca^{2+} channel mutant

The ka901 mutation lies in the pore-forming region of the $InsP_3R$ and RyanR families among which a putative pore-forming motif GXRXGGGI/VGD (the G2630 residue of the $DmInsP_3R$ mutated in ka901 is underlined) is highly conserved. Mutational studies of the homologous G4826 residue in RyanR2 has shown that the G4826C mutant does not form functional homomeric channels in bilayer experiments (Chen et al., 2002), similar to what we observe with ka901 homomeric channels. The absence of functional channels from ka901 homomers in bilayer experiments agrees with the genetic finding that the allelic strength of ka901 is equivalent to that of the null allele 90B0 (Joshi et al., 2004). To understand why microsomal vesicles from *ka901*/+ heterozygotes release greater amounts of Ca^{2+}, co-infection with wild-type $DmInsP_3R$ and ka901 studies can be done similar to what has been done with RyanR2-G4826C to obtain hybrid channels (Chen et al., 2002; Zhao et al., 1999). These experiments are currently in progress.

CONCLUSION

Genetic and biophysical approaches to the $InsP_3R$ structure-function

In conclusion, single-channel properties of embryonic and adult head splice variants of the *Drosophila* $InsP_3R$ (Sinha and Hasan, 1999) and three previously isolated and

sequenced *Drosophila* InsP$_3$R point mutants (Deshpande et al., 2000; Joshi et al., 2004) have been characterized in our study. Our results indicate that the main functional properties of InsP$_3$R are conserved in evolution from DmInsP$_3$R to InsP$_3$R1 (Table 1) and furnish further evidence for differences in function between splice variant isoforms. Changes in the DmInsP$_3$R properties induced by random mutagenesis have helped identify residues that may not necessarily be identified easily by a targeted mutagenesis approach. Although one of these residues (ka901) in homomeric state supports the data obtained earlier from a similar mutation in the RyanR2 (Chen et al., 2002), the others provide fresh insights into the mechanism of Ca^{2+} dependence and the relationship between ligand binding and gating. Furthermore, the single-channel properties of the wild-type and mutant DmInsP$_3$Rs have been correlated with characteristics of InsP$_3$-dependent Ca^{2+} fluxes supported by these channels in experiments with microsomes from wild-type and mutant *Drosophila*. The approaches used in this work have thus allowed for the extension of genetic studies of the InsP$_3$R in a model organism to biophysical studies on the channel.

We thank Tie-Shan Tang for assistance with biochemical experiments, and Phyllis Foley for expert administrative assistance.

S.S.'s visit to Dallas was supported by the Journal of Cell Science Traveling Fellowship. I.B. is supported by the Robert A. Welch Foundation and the National Institutes of Health (R01 NS38082). G.H. is supported by a grant from the Department of Science and Technology and core grants from the National Centre for Biological Sciences, Tata Institute of Fundamental Research, Bangalore, India.

REFERENCES

Berridge, M. J. 1993. Inositol trisphosphate and calcium signalling. *Nature*. 361:315–325.

Bezprozvanny, I., and B. E. Ehrlich. 1995. The inositol 1,4,5-trisphosphate (InsP$_3$) receptor. *J. Membr. Biol.* 145:205–216.

Bezprozvanny, I., J. Watras, and B. E. Ehrlich. 1991. Bell-shaped calcium-response curves of $Ins^{1,4,5}P_3$- and calcium-gated channels from endoplasmic reticulum of cerebellum. *Nature*. 351:751–754.

Boehning, D., and S. K. Joseph. 2000. Direct association of ligand-binding and pore domains in homo- and heterotetrameric inositol 1,4,5-trisphosphate receptors. *EMBO J.* 19:5450–5459.

Boehning, D., D. O. Mak, J. K. Foskett, and S. K. Joseph. 2001. Molecular determinants of ion permeation and selectivity in inositol 1,4,5-trisphosphate receptor Ca^{2+} channels. *J. Biol. Chem.* 276:13509–13512.

Bosanac, I., J. R. Alattia, T. K. Mal, J. Chan, S. Talarico, F. K. Tong, K. I. Tong, F. Yoshikawa, T. Furuichi, M. Iwai, T. Michikawa, K. Mikoshiba, and M. Ikura. 2002. Structure of the inositol 1,4,5-trisphosphate receptor binding core in complex with its ligand. *Nature*. 420:696–700.

Bramley, T. A., G. S. Menzies, and T. Jowett. 1990. Specific binding sites for 125I-labelled human luteinizing hormone (hLH) in microsomal fractions from *Drosophila*. *Mol. Cell Endocrinol.* 73:93–104.

Chen, S. R., P. Li, M. Zhao, X. Li, and L. Zhang. 2002. Role of the proposed pore-forming segment of the Ca^{2+} release channel (ryanodine receptor) in ryanodine interaction. *Biophys. J.* 82:2436–2447.

Deshpande, M., K. Venkatesh, V. Rodrigues, and G. Hasan. 2000. The inositol 1,4,5-trisphosphate receptor is required for maintenance of olfactory adaptation in *Drosophila* antennae. *J. Neurobiol.* 43:282–288.

Furuichi, T., K. Kohda, A. Miyawaki, and K. Mikoshiba. 1994. Intracellular channels. *Curr. Opin. Neurobiol.* 4:294–303.

Hasan, G., and M. Rosbash. 1992. *Drosophila* homologs of two mammalian intracellular Ca^{2+}-release channels—identification and expression patterns of the inositol 1,4,5-triphosphate and the ryanodine receptor genes. *Development.* 116:967–975.

Joshi, R., K. Venkatesh, R. Srinivas, S. Nair, and G. Hasan. 2004. Genetic dissection of *Itpr* gene function reveals a vital requirement in aminergic cells of *Drosophila* larvae. *Genetics.* 166:225–236.

Kaznacheyeva, E., V. D. Lupu, and I. Bezprozvanny. 1998. Single-channel properties of inositol (1,4,5)-trisphosphate receptor heterologously expressed in HEK-293 cells. *J. Gen. Physiol.* 111:847–856.

Lupu, V. D., E. Kaznacheyeva, U. M. Krishna, J. R. Falck, and I. Bezprozvanny. 1998. Functional coupling of phosphatidylinositol 4,5-bisphosphate to inositol 1,4,5-trisphosphate receptor. *J. Biol. Chem.* 273:14067–14070.

Mathew, M. K., R. Nagaraj, and P. Balaram. 1982. Ionophore-mediated transmembrane movement of divalent cations in small unilamellar liposomes: an evaluation of the chlortetracycline fluorescence technique and correlations with black lipid membrane studies. *J. Membr. Biol.* 65:13–7.

Mignery, G. A., and T. C. Sudhof. 1990. The ligand binding site and transduction mechanism in the inositol-1,4,5-triphosphate receptor. *EMBO J.* 9:3893–3898.

Miyakawa, T., A. Maeda, T. Yamazawa, K. Hirose, T. Kurosaki, and M. Iino. 1999. Encoding of Ca^{2+} signals by differential expression of IP^3 receptor subtypes. *EMBO J.* 18:1303–1308.

Miyakawa, T., A. Mizushima, K. Hirose, T. Yamazawa, I. Bezprozvanny, T. Kurosaki, and M. Iino. 2001. Ca^{2+}-sensor region of IP^3 receptor controls intracellular Ca^{2+} signaling. *EMBO J.* 20:1674–1680.

Myers, E. W., G. G. Sutton, A. L. Delcher, I. M. Dew, D. P. Fasulo, M. J. Flanigan, S. A. Kravitz, C. M. Mobarry, K. H. Reinert, K. A. Remington, E. L. Anson, R. A. Bolanos, H. H. Chou, C. M. Jordan, A. L. Halpern, S. Lonardi, E. M. Beasley, R. C. Brandon, L. Chen, P. J. Dunn, Z. Lai, Y. Liang, D. R. Nusskern, M. Zhan, Q. Zhang, X. Zheng, G. M. Rubin, M. D. Adams, and J. C. Venter. 2000. A whole-genome assembly of *Drosophila*. *Science.* 287:2196–2204.

Nosyreva, E., T. Miyakawa, Z. Wang, L. Glouchankova, A. Mizushima, M. Iino, and I. Bezprozvanny. 2002. The high affinity calcium-calmodulin-binding site does not play a role in modulation of type 1 inositol (1,4,5)-trisphosphate receptor function by calcium and calmodulin. *Biochem. J.* 365:659–667.

Nucifora, F. C., Jr., S. H. Li, S. Danoff, A. Ullrich, and C. A. Ross. 1995. Molecular cloning of a cDNA for the human inositol 1,4,5-trisphosphate receptor type 1, and the identification of a third alternatively spliced variant. *Brain Res. Mol. Brain Res.* 32:291–296.

Ramos-Franco, J., D. Galvan, G. A. Mignery, and M. Fill. 1999. Location of the permeation pathway in the recombinant type 1 inositol 1,4,5-trisphosphate receptor. *J. Gen. Physiol.* 114:243–250.

Sinha, M., and G. Hasan. 1999. Sequencing and exon mapping of the inositol 1,4,5-trisphosphate receptor cDNA from *Drosophila* embryos suggests the presence of differentially regulated forms of RNA and protein. *Gene*. 233:271–276.

Swatton, J. E., S. A. Morris, F. Wissing, and C. W. Taylor. 2001. Functional properties of *Drosophila* inositol trisphosphate receptors. *Biochem. J.* 359:435–441.

Tang, T.-S., H. Tu, E. Y. Chan, A. Maximov, Z. Wang, C. L. Wellington, M. R. Hayden, and I. Bezprozvanny. 2003a. Huntingtin and huntingtin-associated protein 1 influence neuronal calcium signaling mediated by inositol-(1,4,5) triphosphate receptor type 1. *Neuron.* 39:227–239.

Tang, T. S., H. Tu, Z. Wang, and I. Bezprozvanny. 2003b. Modulation of type 1 inositol (1,4,5)-trisphosphate receptor function by protein kinase A and protein phosphatase 1α. *J. Neurosci.* 23:403–415.

Taylor, C. W. 1998. Inositol trisphosphate receptors: Ca^{2+}-modulated intracellular Ca^{2+} channels. *Biochim. Biophys. Acta.* 1436:19–33.

Thrower, E. C., R. E. Hagar, and B. E. Ehrlich. 2001. Regulation of Ins(1,4,5)P_3 receptor isoforms by endogenous modulators. *Trends Pharmacol. Sci.* 22:580–586.

Tu, H., T. Miyakawa, Z. Wang, L. Glouchankova, M. Iino, and I. Bezprozvanny. 2002. Functional characterization of the type 1 inositol 1,4,5-trisphosphate receptor coupling domain SII(+/−) splice variants and the *opisthotonos* mutant form. *Biophys. J.* 82:1995–2004.

Tu, H., E. Nosyreva, T. Miyakawa, Z. Wang, A. Mizushima, M. Iino, and I. Bezprozvanny. 2003. Functional and biochemical analysis of the type 1 inositol (1,4,5)-trisphosphate receptor calcium sensor. *Biophys. J.* 85: 290–299.

Uchida, K., H. Miyauchi, T. Furuichi, T. Michikawa, and K. Mikoshiba. 2003. Critical regions for activation gating of the inositol 1,4,5-trisphosphate receptor. *J. Biol. Chem.* 278:16551–16560.

Venkatesh, K., and G. Hasan. 1997. Disruption of the IP3 receptor gene of *Drosophila* affects larval metamorphosis and ecdysone release. *Curr. Biol.* 7:500–509.

Wagner 2nd, L. E., W. H. Li, and D. I. Yule. 2003. Phosphorylation of type-1 inositol 1,4,5-trisphosphate receptors by cyclic nucleotide-dependent protein kinases: a mutational analysis of the functionally important sites in the S_{2+} and S_{2-} splice variants. *J. Biol. Chem.* 278:45811–45817.

Yoshikawa, F., H. Iwasaki, T. Michikawa, T. Furuichi, and K. Mikoshiba. 1999. Cooperative formation of the ligand-binding site of the inositol 1,4,5-trisphosphate receptor by two separable domains. *J. Biol. Chem.* 274:328–334.

Yoshikawa, F., M. Morita, T. Monkawa, T. Michikawa, T. Furuichi, and K. Mikoshiba. 1996. Mutational analysis of the ligand binding site of the inositol 1,4,5-trisphosphate receptor. *J. Biol. Chem.* 271:18277–18284.

Yoshikawa, S., T. Tanimura, A. Miyawaki, M. Nakamura, M. Yuzaki, T. Furuichi, and K. Mikoshiba. 1992. Molecular cloning and characterization of the inositol 1,4,5-trisphosphate receptor in *Drosophila melanogaster*. *J. Biol. Chem.* 267:16613–16619.

Zhao, M., P. Li, X. Li, L. Zhang, R. J. Winkfein, and S. R. Chen. 1999. Molecular identification of the ryanodine receptor pore-forming segment. *J. Biol. Chem.* 274:25971–25974.